Electron Emission from the Electronic States of Oxygen Precipitates in Oxygen-Implanted Silicon

Denis Danilov,* Oleg Vyvenko, Anton Loshachenko, and Nikolay Sobolev

Defect structure and electric properties of n-type silicon samples subjected to multienergy oxygen implantation and subsequent multistage thermal treatments at different high temperatures and durations are investigated with the help of transmission electron microscopy (TEM), capacitance–voltage ($C(V)$), and deep level transient spectroscopy (DLTS) techniques. Well spatially separated layers in the depth consisting of three predominant types of defects—threading dislocations (TDs), oxygen precipitates (OPs) together with diverse extended structural defects and OPs only—are observed with TEM. While the properties of DLTS spectra from the layer with TDs coincide well with dislocation-related ones reported in numerous previously published articles, the spectra from the OP layer are found to show unusual distinct property: the low-temperature tail of DLTS peak does not or very weakly depend on the rate window. A simplified semi-quantitative model is proposed based on a big positive charge of OP layer revealed from $C(V)$ measurements. The model explains the unusual property to be due to an increase of the Coulomb-like attractive potential upon electron emission from the electronic states of the OPs giving rise to logarithmic emission kinetics.

1. Introduction

Oxygen precipitates (OPs) are commonly used in silicon microelectronics to clean the active region of wafers from undesirable interstitial metal impurities. This process, called "internal gettering," is based on the ability of the OPs to capture impurity atoms from the silicon environment.[1] OPs are surrounded by lattice deformation fields and their growth is accompanied by injection of self-interstitials leading to creation of punch-out dislocations and stacking faults owning the local electronic levels in the

D. Danilov, A. Loshachenko
Interdisciplinary Research Center for Nanotechnology
Saint-Petersburg State University
Universitetskaya emb. 7/9, St. Petersburg 199034, Russia
E-mail: d.danilov@spbu.ru

O. Vyvenko
Faculty of Physics
Saint-Petersburg State University
Universitetskaya emb. 7/9, St. Petersburg 199034, Russia

N. Sobolev
Department of Solid State Electronics
Ioffe Institute
Polytekhnicheskaya 26, St. Petersburg 194021, Russia

The ORCID identification number(s) for the author(s) of this article can be found under https://doi.org/10.1002/pssa.202100662.

silicon bandgap affecting greatly the recombination of excess carriers. The studies of OPs electric and recombination properties in silicon have a long history.

In 1986, Hwang and Schroder[2] demonstrated that OPs are mainly responsible for the observed carrier lifetime degradation and that recombination at OPs takes place through Si/OP interface states. In addition, they found that the lifetime degradation is more severe in p-Si than in n-Si even for identical densities and sizes of OPs. A model for recombination at OPs was presented in terms of the surface recombination velocity at the Si/OP interface. To explain the lifetime difference between n-Si and p-Si, they propose a band bending around OPs caused by positive fixed charges in the OPs. A broad deep level transient spectroscopy (DLTS) spectra caused by the carrier emission from Si/OP interface states were found to be similar to conventional Si/SiO$_2$ interface states which, depending on the conditions of heat treatment, forms the energetic bands with monotonically increasing density toward permitted band edges as well as a deep level at $E_c - 0.45$ eV. Besides, transmission electron microscopy (TEM) studies revealed the presence of dislocation loops and stacking faults near few largest OPs, but their influence on the DLTS spectra was believed to be negligible.

The formation of OPs with punched out loops and dislocations was also shown by Whitfield et al.[3] in oxygen-contained silicon with a two-stage high-temperature treatment. However, instead of broad energy state distribution, the two main energy levels for the carrier traps, with the energy positions $E_c - 0.41$ eV, $E_c - 0.23$ eV, and capture cross sections 10^{-14} cm^2 and 7×10^{-16} cm^2 were found.

Similar deep electron states with $E_c - 0.4$ eV and $E_c - 0.3$ eV were found later by Schmalz et al.[4] in the study of n-Cz-Si after a long heat treatment in the temperature range from 600 to 900 °C. A mixture of the perfect dislocation loops, stacking faults, and OPs was observed in TEM making impossible an identification of the states and it was proposed that the first level was related to a certain stage of the oxygen precipitate growth, and the second one to a high density of dislocation loops.

Koizuka and Yamada-Kaneta[5] showed the formation of resembling OP-related state ($E_c - 0.3$ eV) with another one ($E_c - 0.25$ eV) in Cz-Si under the multistage thermal treatment in the temperature range from 500 to 1100 °C. The authors noted that the observed distribution and the temperature dependence

of the traps density are very similar to that of the well-known P_b center formed at Si—SiO$_2$ interface.

Vanhellemont et al.,[6] studying the electrical activity of extended lattice defects formed by oxygen precipitation in silicon under the multistage annealing, found two electron states with energies $E_c - 0.43$ eV and $E_c - 0.23$ eV. The formation of precipitation-related defects, precipitate/dislocation complexes, isolated plate-like SiO$_x$ precipitates, and small bulk stacking faults with a central OP, was revealed with TEM. The authors noted the presence of leakage current in the samples, which was later investigated in detail by Murakami,[7] who showed their relation with oxygen-related defects.

DLTS study of traps introduced in p-Cz-Si wafers during two-step annealing procedures in 1999 was published by Mchedlidze et al.[8] The authors observed two majority carrier traps $E_V + 0.43$ eV and $E_V + 0.26$ eV, which were assigned to the plate-like silicon oxide precipitate surface and the punch-out dislocations, respectively. Two minority carrier traps at the $E_c - 0.42$ eV and $E_c - 0.22$ eV were found as well consistent with the above-listed published results.

Kot et al.[9] investigated the evolution of the electron states in n-Cz-Si samples with an increase of the annealing temperature and found an additional shallow level $E_c - 0.16$ eV that was attributed to rod-like defects accompanied by OPs growth process. Such an OP-related level was also reported by Tejada et al.[10]

The main problem in the trap identification is the common coexistence of OPs and of the surrounding defects, caused by OPs growth such as punch-out dislocations, etc. As the sizes of such conglomerates are much smaller than the characteristic width of space-charge region (SCR) of the diodes, the states of all defects contribute to the measured signal.

Recently, Danilov et al.[11–14] in a series of investigations of oxygen-implanted silicon samples found that, by a suitable choice of the implantation energies and subsequent high-temperature treatments, the regions with a high density of dislocations and of OPs could be spatially separated in the depth and were located within the SCR of Schottky diodes or p–n junctions. These enabled to distinguish electrical properties of the OPs and other structural defects by varying the voltages applied to the diodes. It was shown that the form of DLTS peaks and the thermoemission activation energies of the electronic levels of OPs and dislocations significantly differed and that, in contrast to dislocation-related states, the electrical properties of the OP states are very sensitive to the treatment conditions. In particular, it was demonstrated that the OP-rich layers of the samples become strongly positively charged at high reverse bias voltages when the OP-related states are emptied from electrons[15] which confirmed the assumption of Hwang and Schroder[2] made from comparison of the minority lifetimes in different types of the samples.

Direct measurements of the OP positive charge values combined with the TEM data on average size and the density of the precipitates revealed a regularity[14] which led to the conclusion that the positive charge is localized within the shells of OPs. This correlates well with the OPs internal structure discovered by Kot et al.,[16,17] which consists of the internal stoichiometric SiO$_2$ core surrounded by a shell of nonstoichiometric SiO$_x$ similar to the oxide layer on the bulk silicon wafer.

That property is opposite to dislocation-related states in which n-type semiconductors are characterized by high-density local acceptor-like states, i.e., neutral in an electron-free state.[18,19] As a result, when they are started to be filled with electrons, a barrier arises that limits the further filling. The barrier does not affect the emission rate but leads to a logarithmic dependence of energy levels occupancy on the refilling time duration and the logarithmic kinetics of the electron capture is commonly served as a fingerprint for the dislocation-related states.

OPs are also multielectron but positively charged defects and no retardation of the electron capture kinetics is expected. In quasineutral n-type silicon, the charge will be compensated by the electrons captured by OPs energy states. In the process of the electron emission from initially neutral OPs, the positive charge increases. As a result, the attractive potential for electrons should increase slowing down of the electron emission rate with the emission time. In turn, such character of the emission transient should be reflected not only in a particular shape of DLTS peak but also in its behavior upon rate window variation conventionally used to retrieve temperature dependence of the emission rate. However, to the best of our knowledge the window dependence for OP-related DLTS peak has not been reported in any of published articles.

In this work, which is a continuation of the previous ones, we investigated in more details the characteristic differences between the properties of DLTS signals from OPs and from dislocations. We will show that a characteristic feature of the DLTS signal from OPs states is weak dependence or independence of the temperature position of the low-temperature tail of the DLTS peak on the rate window. We propose a simplified theoretical model that explains such behavior by logarithmic type kinetics of the electrons emission from the OPs states.

2. Extended Defect Structure and Charge Distribution in the Implantation Region

Figure 1 shows a TEM image of the cross-sectional near-surface region of the sample. Careful examination of the microgram
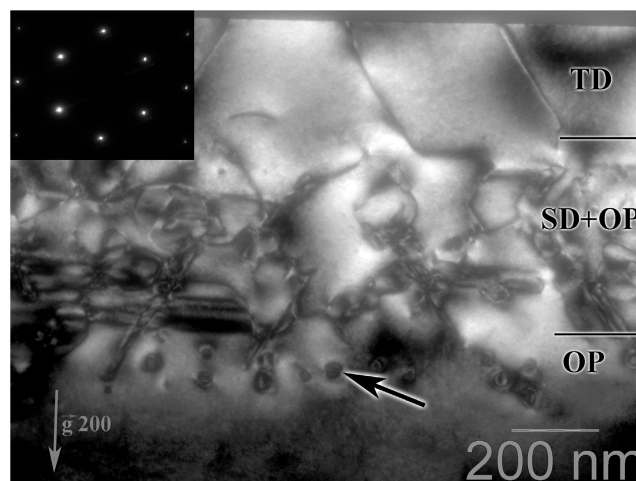

Figure 1. Dark-field cross-sectional TEM image of implantation region. The diffraction patterns are shown in the inset. Three layers marked as TD, SD + OP, and OP are clearly differed by their dominated type of the extended defects. The black arrow shows one of the big OPs.

reveals that the extended defect structure in the investigated samples can be characterized by three characteristic layers. In the near-surface area of implantation at a depth of down to 200 nm, where according to SRIM data the oxygen concentration is rather low, threading dislocations (TDs) of a density of about 10^{10} cm^{-2} prevailed (in the image marked as "TD"); at the depths from 200 to 700 nm, a lot of structural defects accompanied with rare small OPs dominated (in the image marked as "SD + OP"), and a homogeneous thin layer of OPs (in the image marked as "OP") was at the back side of the implantation region at a depth of ≈800 nm. The density of big precipitates in the OP layer as obtained from multiple TEM images was of about 0.9×10^{10} cm^{-2}.

Figure 2 shows the $C^{-2}(V)$ characteristics recalculated from high-frequency $C(V)$ measurements at two selected temperatures of 100 and 200 K of the sample. The chosen temperatures correspond (200 K) or well below (100 K) to the position OP-related DLTS peak (see next section). Above the reverse bias voltage values $U = -5$ V, the curves demonstrate a linear dependence on the voltage expected for a uniformly doped semiconductor with a net shallow donor density of few 10^{15} cm^{-3}. Besides, two regions with a reduced slope below $U = -1$ V and in the some ranges around $U = -4$ V correspond to an increased net-donor concentration that is clearly visible in the concentration profiles of Figure 2b. A comparison of the SCR depths, calculated from the capacitance values, with the depths of the characteristic defect layers in TEM image Figure 1 reveals that the monotonic increase of net-donor concentration to the surface corresponds to the SCR depths within the SD + OP region while the sharp peaks near a SCR depth of about 0.8 μm coincides well with the location of the narrow OP-rich layer at the bottom of the implanted region. The sharp peak on the concentration profile shown in Figure 2b for two temperatures was observed also in the entire interval between 50 and 300 K (not shown all for clarity), indicating a temperature-independent electron exchange. This implies that its origin is not due to Fermi-level pinning by the refilling of deep levels but rather due to enhancement of the free electron density in accordance with the fact that differential capacitance measurements provide not the profile of the impurity atom distribution but, instead, that of the majority carrier distribution.[20]

One should note that the width of the OP concentration peak at 200 K is less than Debye length, L_D, at that temperature (100 nm) and the peak position shifts to the depth as temperature decreases down to 100 K following L_D decrease. This might be explained due to the limited resolution of $C(V)$ profiling defined by the L_D value. As was pointed out by Wu et al.[21] in the case of such narrow impurity distribution with an abrupt concentration profile, the incremental charge associated with the applied testing voltage is spread over a wider region than the half-width of the profile that gives rise to noticeable deviation of the profile calculated based on depletion approximation from true one. An algorithm of the recalculation of $C(V)$ data into free electron concentration proposed in the study by Kennedy et al.[20] was shown to give also erroneous results for abrupt profiles[22] and the numerical solution of Poisson equation could not help much in our case due to the lack of the exact knowledge of the initial charge distribution.

An alternative way to estimate the charge within the inhomogeneously doped region is to utilize the general relationship between the potential of a diode and the charge distribution within SCR

$$V = \frac{1}{\varepsilon\varepsilon_0} \int_0^w (q\Delta N_Q(x) + qN_D)x\,dx$$

$$= \frac{1}{\varepsilon\varepsilon_0} \int_0^w q\Delta N_Q(x)x\,dx + \frac{qN_D}{2\varepsilon\varepsilon_0}w^2 \qquad (1)$$

where N_D is the uniform donor density in reference sample, $\Delta N_Q(x)$ is the additional charge density introduced in the investigated implanted sample, $\varepsilon\varepsilon_0$ are the relative and absolute permittivity, and q is the elemental charge. In this way, the geometrical capacitance of the structure per area unit will be

$$C = \sqrt{\frac{\varepsilon\varepsilon_0 qN_d}{2(V - \Delta V)}} \qquad (2)$$
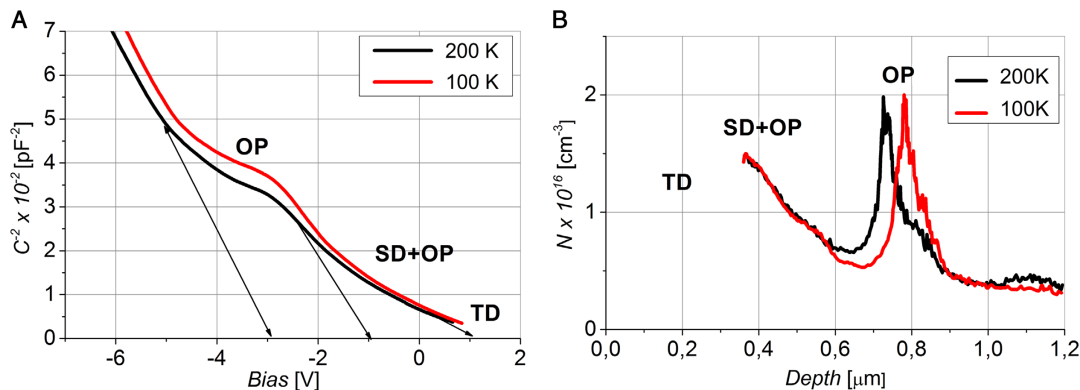
where

Figure 2. a) $C^{-2}(V)$ dependence at a characteristic temperature of 200 K (black line) and 100 K (red line). b) Net-donor concentration profiles at 200 K (black line) and 100 K (red line). Approximate positions of three layers with well-distinguished defect structure are marked in compliance with TEM image in Figure 1.

$$\Delta V = \frac{1}{\varepsilon \varepsilon_0} \int_0^w q \Delta N_Q(x) x dx \qquad (3)$$

$$V = V_{appl} + V_{diff}$$

where V_{appl} is the applied external voltage and V_{diff} is the diffusion voltage of p–n junction.

For the particular of $C(V)$ profile in Figure 2b, the latter can be divided into a contribution of a thin layer with a plane-like charge distribution of an area density N_s at the depths x_0 and the region with an increased additional charge density $\Delta N_Q(x)$ between the depths 0 and x_s giving rise to

$$\Delta V = \Delta V_{2D} + \Delta V_{surf}$$

$$\Delta V_{surf} = \frac{1}{\varepsilon \varepsilon_0} \int_0^{xs} q \Delta N_Q(x) x dx \qquad (4)$$

$$\Delta V_{2D} = \frac{q N_s x_0}{\varepsilon \varepsilon_0}$$

This expression provides a way to evaluate N_s from the changes of the effective built-in voltage obtained as the cutoffs of extrapolated linear parts of $C^{-2}(V)$ to the voltage coordinates.

An examination of the data of Figure 2a shows that within the forward bias ranges the built-in voltage is of about 1 V being close to the expected value for asymmetric p–n junction while the part above $U = -5$ V results in big negative values reflecting a big positive charge formed within fully depleted SCR due to electron escape. The area positive charge density of OP layer was calculated from the difference between the cutoff voltages above and below the plateau shown by arrowed lines in Figure 2a with the help of Equation (3) as

$$N_s = \frac{\varepsilon \varepsilon_0 \Delta V2_D}{q x_0} \qquad (5)$$

Giving for $x_0 = 0.8\,\mu m$ an approximate value of N_s of about $2 \times 10^{11}\,cm^{-2}$. Nearly the same value was obtained from the integration of the OP peak on the free electron concentration profile Figure 2b. Taking the precipitate density from TEM of about $10^{10}\,cm^{-2}$, an average precipitate charge can be estimated to be about 20 electron charges.

3. DLTS Signal Behavior at Different Depths

Figure 3 shows the DLTS spectrum of the sample for diverse rate windows shown in the legend. The offset voltage applied to the diodes in the experiment was −1.5 V; the voltage of the refilling pulses was +1 V. The selected parameters correspond to the response of the level located from the surface to 0.4 μm–λ, where

$$\lambda = \sqrt{\frac{2 \varepsilon \varepsilon_0 (E_t - E_F)}{q N_d}} \qquad (6)$$

is the distance from the intersection point of the level, E_t with the quasi-Fermi level, and E_F with respect to the SCR edge. The latter value was difficult to calculate exactly due to strong inhomogeneity of the apparent net-donor concentration but it is roughly
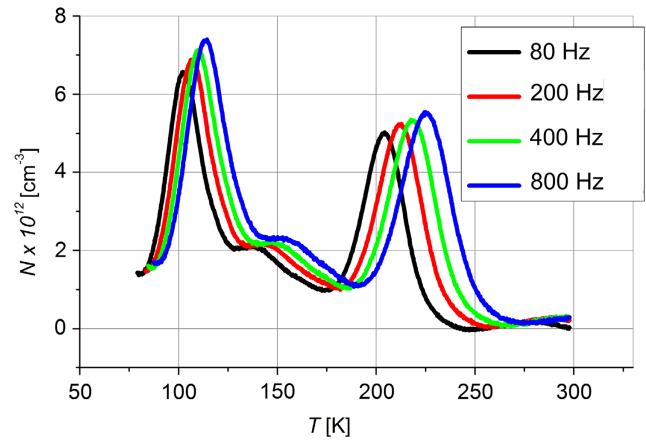

Figure 3. DLTS spectra from dislocation deep levels. Reverse bias voltage and refilling pulse voltage were −1.5 and +1 V, respectively. The rate windows are shown in legends.

of the order of 0.1–0.2 μm for the $10^{16}\,cm^{-3}$ donor density for all observed levels and temperatures. This implies that the electron emission stems predominantly from the layer TD with a high density of threading dislocations with a minor contribution of the SD + OP layer boarder. The spectrum shows three main peaks at temperatures of ≈100, ≈150, and ≈200 K and looks like very similar to the reported by Omling et al.[19] in plastically deformed silicon. Two most intensive DLTS peaks at 100 and 200 K possessed logarithmic capture kinetics being a characteristic feature of acceptor-like extended defect. Their activation energies for electron emission and electron capture cross sections as defined from DLTS peak temperature shift ($E_c - E_t = 0.18$ eV, $\sigma = 3 \times 10^{-15}\,cm^2/E_c-E_t = 0.39$ eV, $\sigma = 1.2 \times 10^{-15}\,cm^2$) coincided well with those of dislocation-related states reported previously in numerous studies and notated first as A in Omling et al.[19] and DE2 in Kveder et al.,[18] respectively. The parameters of the not well-resolved peak at 150 K was not possible to determine but its temperature position coincided with the peak marked as B in Omling et al.[19] Thus, we are believed in the dislocation origin of the electronic states in the near-surface region of our samples.

Figure 4 shows the DLTS spectra of sample measured at −6 V bias and −4 V pulse voltage level. These voltages correspond to the electron emission from the states located in the OP layer OP at the back side of the implantation region responsible for the concentration peak in Figure 2b. The spectrum has a main broadband with a peak temperature within the ranges between 150 and 250 K. One can note also a small hillock near 150 K that coincided well with the dislocation-related low-temperature DLTS peak (see Figure 3) and is due to a contribution from the traps in the SD + OP layer.

The big temperature breadth of the band is consistent with the previously published properties of OP-related DLTS signal. But the band possesses other distinct feature. That is its unusual behavior under variation of the rate window. Instead of a regular shift of the peak with the temperature as a whole, as it follows from the theory of DLTS technique and like it was observed for dislocation-related states in Figure 3, the low-temperature tail of the peak does not move practically with
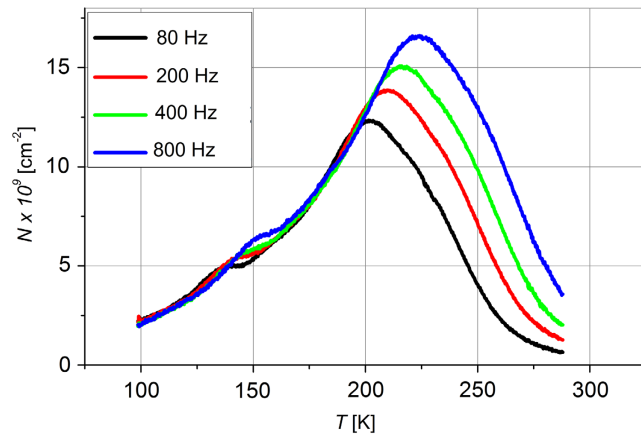
Figure 4. DLTS spectra of the sample measured at reverse bias voltage and refilling pulse voltage were -6 and $-4\,V$, respectively. The rate windows are shown in legends.

Figure 5. DLTS spectra of the sample measured at reverse bias voltage and refilling pulse voltage were -5 and $-4\,V$, respectively. The rate windows are shown in legends. Inset compares DLTS spectra at reverse biases voltage/refilling pulse voltage of $-5\,V/-4\,V$ and $-6\,V/-4\,V$ for 800 Hz rate windows.

the rate window while its high-temperature tail shows an usual behavior giving from Arrhenius plot the values $E_c - E_t = 0.38\,eV$, and $\sigma_n = 1.7 \times 10^{-15}\,cm^{-2}$.

The peak magnitude was rather high being about 10% of the basic capacitance well exceeding the dislocation-related signal from TD layer but, nevertheless, it maintains the linear relationship between the emitted charge and capacitance changes. Thus, the observed unusual behavior of the OP-related DLTS peak could not be explained as an artifact due to break off of the validity of conventional DLTS approximation.

As the OP-related states are localized in a narrow layer, the area density was calculated according to

$$N_s = N_d \frac{S^2(\varepsilon\varepsilon_0)^2}{x_0} \frac{\Delta C}{C^3} \qquad (7)$$

The peak value of the DLTS signal due to recharging the traps in the OP layer corresponds to a density of about $10^{10}\,cm^{-2}$ which is an order of magnitude less than the total density obtained from C(V) data. This is believed due to the nonexponential character of the electron emission kinetics leading also to the broadening of the DLTS line.

Figure 5 shows the second example of DLTS spectra from the OP layer measured at a lower reverse bias of $-5\,V$ than shown in Figure 4 and the same refilling pulse voltage of $-4\,V$. The spectrum is very similar to the previous one and contains of a hillock at 150 K from dislocation states the $SD + OP$ region that distinctly shifted under rate window variation and a broad OP-related DLTS band whose low-temperature tails coincide for all rate window used. The emission parameters as retrieved from the temperature values of the OP-related peak were $E_c - E_t = 0.33\,eV$ and $\sigma_n = 3.2 \times 10^{-16}\,cm^{-2}$. The inset in Figure 5 demonstrates the changes in the OP-related DLTS band under reverse bias voltage changes for the selected 800 Hz rate window. One can note that, with the increase in the reverse bias gives rise not only to expected increase of the signal but also to a shift of the band to a high temperature.
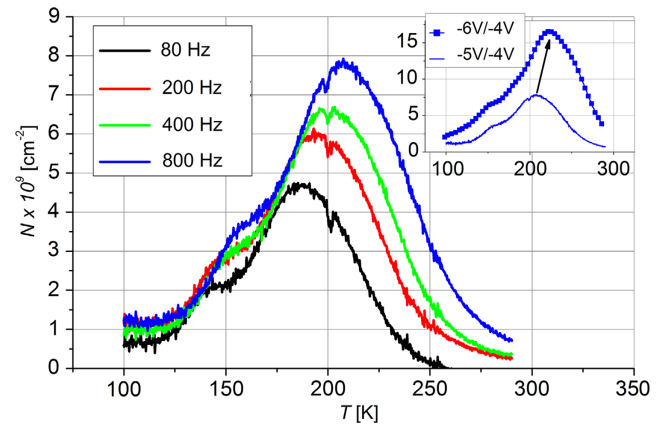
4. Discussion

Experimental results presented above revealed the presence of a large positive charge confined in a thin layer situated at the depth corresponding to the position of a high concentration of oxygen precipitates. Besides, it was found that the behavior of OP-related DLTS peaks noticeably differs from theoretically predicted and commonly observed regular shift of the peaks as a whole under the variation of the rate window, which also was demonstrated in the investigated samples for dislocation-related electronic states. The main unusual property of DLTS peaks due to OP is the independence of low-temperature tail on the rate window. In particular conditions of our experiments, DLTS signal was measured as the capacitance transient difference between the time points t_1 and t_2 keeping the ratio t_2/t_1 constant. The only function that is independent on such ratio is logarithmic one. Logarithmic type kinetics is well known for the carrier capture with the initially neutral states of multielectron extended defects like dislocations and transition metal silicide precipitates in silicon (see Introduction for refs.). It is caused by an increase of the capture barrier which is proportional to the increase of the total charge of the defects. This gives a hint that the logarithmic kinetics of the emission can be caused by an increase of the emission barrier upon emptying of the OP states from electrons that is due to an increase of their positive charging.

The positive charge of a single OP, qZ, in our samples was estimated to be of the order 20 electron charges forming, thus a potential well attractive for electrons.

When OPs are situated in the quasi-neutral region of the diode, their potential wells will be populated with free electrons. The electrons can remain free or be captured at the interface states. In the first case, in a simple model the potential can be described with the help of screened Coulomb potential of a point charge, or Yukawa potential, that assumes proportionality between potential and free electron density

$$U = \frac{qZ}{4\pi\varepsilon\varepsilon_0 r} e^{-r/L_D} \qquad (8)$$

where

$$L_D = \sqrt{\frac{\varepsilon\varepsilon_0 kT}{q^2 n}} \quad (9)$$

In Debye screening length, n is the free electron concentration and kT/q is the thermal energy.

For the spherical OP of a radius R_0, the expression of the potential is transformed to

$$U = \frac{qZe^{-(r-R_0)/L_D}}{4\pi\varepsilon\varepsilon_0 r(R_0/L_D + 1)} \quad (10)$$

That can be used to estimate the depth of the well for electrons of neutral OP, i.e. when its states are filled with electrons. For example, the depth of the well, $U(R_0)$, for OP with a diameter of 25 nm in silicon with a free electron concentration of 10^{15} cm^{-3} varies in the temperature range of interest from $9Z$ to $8Z$ that gives for $Z = 20$ $U(R_0) = 160$–180 meV. In the empty state, the potential is Coulomb-like and the depth of the well with the same parameters is rather close to the screened potential case to be of 200 meV.

The electric field at the OP surface surrounded by free electrons

$$E(R_0) = 1.3 x 10^{-8} \frac{Z}{R_0^2} (\text{V cm}^{-1}) \quad (11)$$

gives $E(R_0) = 8 \times 10^3 Z$ (V cm^{-1}). For $Z = 20$, it corresponds to the field of 10^5 V cm^{-1} that exceeded well the typical field value in the SCR of the diode with $n = 10^{15}$ cm^{-3}. This implies that potential well persists in the entire SCR even when it filled with free electrons.

The density of the states at Si–SiO$_2$ interface is known to be typical of the order of 10^{12} cm^{-2}.[2,23] For spherical OP with $R_0 = 25$ nm with a surface area of 2×10^{-11} cm^{-2}, the number of the states is about 20 which is of the order the same that the positive charge estimated above from the experimental data. Thus, one can assume that the electrons when captured in the OP potential well are confined at the interface states between OP and silicon. In this case, one can use nonscreened Coulomb potential to evaluate kinetics of the electron emission from the states.

The energy density of the interface states increases to the c-band edge so that the main contribution should give the rather shallow states.

As the first approximation, we will restrict us with a very simplified model assuming that energy activation for the thermal emission from the neutral OP is negligible. In this way, introducing frequency factor, $\nu(T)$, one can write following rate equation

$$\Delta U(t) = \alpha(Z - N(t))$$
$$\frac{dN}{dt} = -\nu N \exp\left\{-\frac{\Delta U}{kT}\right\} \quad (12)$$

where N is the number of electrons at OP and

$$\alpha = \frac{q}{4\pi\varepsilon R_0} \quad (13)$$

which for OP with a diameter of 25 nm is 10 meV.

The solution of the rate Equation (12) is the integral exponential function in which main term is logarithm and can be solved

exactly only numerically. An approximate solution can be obtained neglecting linear dependence on N with respect to exponential one. In this approximation, the solution with boundary conditions

$$t = 0, \ N = N_0$$
$$t = t, \ N(t) \quad (14)$$

will be

$$N(t) = N_0 - \frac{kT}{\alpha}\ln\left(1 + \frac{\alpha\nu N}{kT}\exp\left\{-\frac{\alpha(Z - N_0)}{kT}\right\}t\right) \quad (15)$$

At the end of the emission process when $\alpha N << kT$

$$\frac{dN}{dt} = -\nu N \exp\left\{-\frac{\Delta U}{kT}\right\} = -\nu\left\{1 + \frac{\alpha N}{kT}\right\}N\exp\left\{-\frac{\alpha Z}{kT}\right\}$$
$$N = \frac{N_0 \exp\left(-\nu\exp\left\{-\frac{\alpha Z}{kT}\right\}t\right)}{1 + \frac{\alpha N_0}{kT}\left[1 - \exp\left(-\nu\exp\left\{-\frac{\alpha Z}{kT}\right\}t\right)\right]} \quad (16)$$

and the emission transient at high temperatures becomes nearly exponential. Thus, one can expect that at low temperatures electron emission kinetics will be logarithmic with the rate window independent DLTS signal while at higher temperature it will transform to usual behavior.

Figure 6 represents DLTS line shapes calculated from the results of exact numerical solution of the rate Equation (14) where frequency factor corresponded to standard expression for thermal emission

$$\nu = \sigma_n v_{th} N_c \exp(-E_{em}/kT) \quad (17)$$

where v_{th} is the electron thermal velocity, N_c is the effective density of states in the conduction band of silicon, electron capture cross section, σ_n, was taken 10^{-15} cm^{-2} and the energy activation of electron thermal emission, $\alpha Z = 125$ or 250 meV (the depth of the potential well in the absence of the electrons), $N_0 = Z$, E_{em} was taken as zero that corresponds to the electrons at the surface states very close to the conduction band. DLTS signal of double-
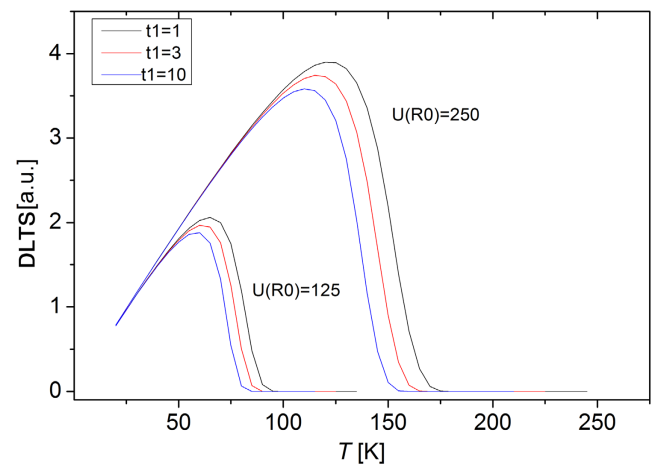

Figure 6. Simulated DLTS spectra according to the rate Equation (14). Double-box correlator with $t_2/t_1 = 10$ and with t_1 in millisecond shown in the legend.

box correlator was calculated as the difference $N(t_1) - N(t_2)$ with $t_2/t_1 = 10$ and with t_1 shown in the legend.

The presented simulated DLTS spectra possess low-temperature tails coincide at different rate windows that reflect the logarithmic type of the transient and that at the lowermost temperatures DLTS signal is also independent on the OP charge in accordance with the approximate solution where the temperature dependence slope is defined by the multiplier at logarithm kT/α depending on α only. The high-temperature tails of the spectra show conventional dependence on the rate window and the activation energy as retrieved from Arrhenius plot coincided with the depth value of the potential well used in calculations.

The decrease of the positive charge value leads to the shift of DLTS peak toward low temperature, as shown in Figure 6. This might explain the low temperature shift with the decrease of the applied reverse bias, Vappl, from -6 V to -5 V observed experimentally and shown in the insert of Figure 5 in the assumption that at $V_{appl} = -5$ V the OP states could not be completely emptied at the end of the emission process as SCR potential value at the OPs position became less than the OP well depth. That corresponds to effective decrease of the OP positive charge and, as a result, to the lowering of the activation energy for electron thermoemission observed experimentally (see inset in Figure 5).

The shape of the simulated spectra is rather similar to the one reported by Hwang and Schroder[2] but, obviously, differs from the experimental spectra presented in this article where a noticeable increase of DLTS signal was observed starting from a certain temperature. This implies that either the emission or capture rate slows down rapidly with the temperature decrease. Generally, an exact model should include many other parameters and variables such as energetic distribution of the interface states and of their cross sections, the diode potential changes due to refilling of OP-related states, a lowering of the emission and capture barriers due to Poole–Frenkel effect and, may be also, the quantization of electron states in the OP potential.

Poole–Frenkel effect can be easily introduced into the calculations but its impact increases with the increase of the positive charge and, obviously, it is most pronounced at the final stage of the emission and cannot help to explain the emission retardation at low temperatures.

Slowdown of the emission rate from the OP states at low temperature could be caused due to participation of sufficiently deep levels in the process as well as due to lowering of the initial level occupation with electrons as a result of strong temperature dependence of electron capture cross section. According to the numerous published data, the density of Si—SiO$_2$ interface state in most cases exponentially increased to the bottom of the conduction band for the bulk samples and OP, exhibiting a maximum at several tens of eV below conduction band.

Regarding the electron capture, an activation dependence for Si—SiO$_2$ interfacial states as a result of multiphonon process was reported in several studies for bulk samples[24,25] while there is no report on such process for OP to the best of our knowledge. The interface states, in fact, are located not immediately on the OP surface but rather within a few atomic layers of nonstoichiometric oxide, and tunneling process is necessary to be included for the electron exchange between the states and conduction band. Then, generally, the expression for capture cross section consists of a tunneling and a thermal activation terms
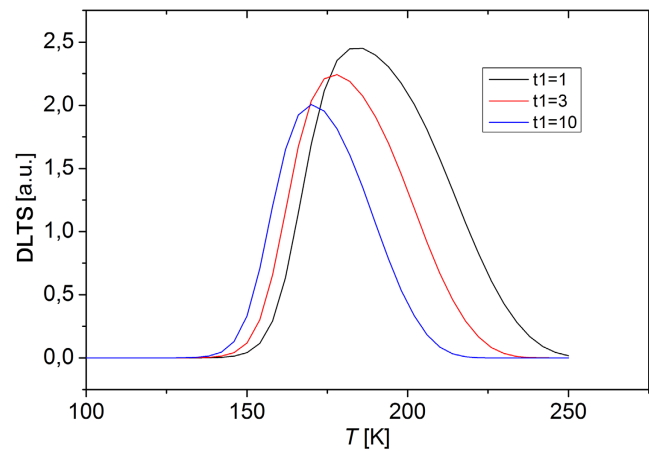

Figure 7. Simulated DLTS spectra according to the modified rate Equation (14) with initial conditions at the end of the refilling pulse of a duration of 1 ms with thermoactivated electron capture cross section. Double-box correlator with $t_2/t_1 = 10$ and with t_1 in millisecond shown in the legend. Details of other input parameters are presented in the text.

$$\sigma_n = \sigma_t + \sigma_\infty \exp(-E_b/kT) \qquad (18)$$

In the DLTS spectra presented in **Figure 7**, following input parameters were used: $E_b = 80$ meV, $\sigma_\infty = 10^{-17}$ cm^{-2}, bulk free electron density $n_0 = 10^{15}$ cm^{-3}, refilling pulse duration 1 ms, energy position of the interface level 30 meV, $\alpha = 10$, Z = 20. As the final occupation of OP states the equality Fermi-level position, $E_f = kT\ln(N_c/n_0)$, with the OP Coulomb energy $\alpha(Z-N)$ was chosen. DLTS signal was calculated as it was described for the calculation of the data for Figure 6.

>One can see that the spectra look quite similar to the experimental one. With an increase of the DLTS peak temperature, their low-temperature tail shifted noticeably slower than the high-temperature one though such close coincidence of the former like in Figure 6 one does not observe. The reason of the discrepancy is not known so far and further improvements of the calculation model are necessary and are in progress now.

One should note also that the activation energy for the thermoemission obtained from Arrhenius plot of the spectra in Figure 6 coincided well with the input value of the well depth used in the calculations while the similar treatment of the spectra in Figure 7 gave the value of 0.4 eV instead of the given input value of 0.3 eV.

5. Conclusion

n-Type silicon samples subjected to multienergy oxygen implantation and subsequent multistage thermal treatments at different high temperatures and durations possess well-separated spatially layers in the depth consisting of three predominant types of defects—threading dislocations, oxygen precipitates together with diverse extended structural defect and oxygen precipitates only as observed with TEM. Capacitance–voltage and DLTS measurement on p–n junction prepared on the samples revealed correlations between the type of the defects and their electric properties. While the properties of DLTS spectra from the layer with threading dislocations

coincided well with dislocation-related ones reported in numerous previously published articles, the spectra from the layers containing oxygen precipitate were found to show unusual distinct behavior: the low-temperature tail of DLTS peak did not or very weakly depend on the rate window. A simplified semiquantitative model was proposed based on the big positive charge of oxygen precipitate layer revealed from capacitance–voltage measurement data in our investigated samples and well-known previous data. The model explains the unusual property to be due to an increase of the Coulomb-like electron emission barrier upon electron emission from the electronic states of the precipitate giving rise to logarithmic-type emission kinetics. Numerical model simulations of DLTS spectra were found in a qualitative agreement with the experimental data and further improvements of the calculation model are necessary to reach a quantitative understanding of the processes.

6. Experimental Section

n-Cz-Si wafer with phosphorus doping concentration of about 10^{15} cm^{-3} was multistage implanted by oxygen with energies of 350/225/150 keV and with doses of $1.5 \times 10^{15}/0.9 \times 10^{15}/0.7 \times 10^{15}$ cm^{-2}, respectively. The sample was subjected to a three-stage heat treatment procedure: 1) at 650 °C for 7 h in Ar ambiance, 2) at 800 °C for 4 h in Ar ambiance; and 3) at 1000 °C for 6 h in chlorine-contained atmosphere (CCA). Secondary mass spectroscopy profiles of oxygen concentration in the samples corresponded rather well to that simulated with SRIM software and consist of near-surface oxygen-poor layer of a thickness 200–250 nm followed by a layer at depths 300–800 nm with a homogeneous oxygen concentration of 5×10^{19} cm^{-3}.[13]

Local p$^+$–n junctions and Ohmic contacts for electrical measurements were formed by vapor-phase epitaxy of polycrystalline silicon highly doped with boron. More detailed description of the sample preparation procedure can be found in the study by Danilov et al.[13]

The sample was characterized with high-frequency (1 MHz) capacitance–voltage, $C(V)$, and DLTS measurements. DLTS measurements were carried out using the SULA Technologies system with a double boxcar correlator in the constant applied voltage mode. The times of the pulses of the convolution signal are related as $t_2 = 5.2 \, t_1$. The repetition period of the refilling pulses and their duration were 50 and 1 ms, respectively.

Conflict of Interest

The authors declare no conflict of interest.

Data Availability Statement

The data that support the findings of this study are available from the corresponding author upon reasonable request.

[1] D. Gilles, E. R. Weber, S. Hahn, *Phys. Rev. Lett.* **1990**, *64*, 196.

[2] J. M. Hwang, D. K. Schroder, *J. Appl. Phys.* **1986**, *59*, 2476.

[3] J. Whitfield, C. J. Varker, S. S. Chan, S. R. Wilson, R. W. Carpenter, S. J. Krause, E. R. Weber, *Advanced Processing and Characterization of Semiconductors III*, Vol. *0623*, SPIE, Bellingham, WA **1986**.

[4] K. Schmalz, F.-G. Kirscht, K. Tittelbach-Helmrich, *Phys. Status Solidi A* **1988**, *109*, 279.

[5] M. Koizuka, H. Yamada-Kaneta, *J. Appl. Phys.* **1998**, *84*, 4255.

[6] J. Vanhellemont, E. Simoen, A. Kaniava, M. Libezny, C. Claeys, *J. Appl. Phys* **1995**, *77*, 5669.

[7] Y. Murakami, Y. Satoh, H. Furuya, T. Shingyouji, *J. Appl. Phys* **1998**, *84*, 3175.

[8] T. Mchedlidze, K. Matsumoto, E. Asano, *Jpn. J. Appl. Phys.* **1999**, *38*, 3426.

[9] D. Kot, T. Mchedlidze, G. Kissinger, W. von Ammon, *ECS J. Solid State Sci. Technol.* **2013**, *2*, P9.

[10] J. A. Jiménez Tejada, A. Godoy, J. E. Carceller, J. A. López Villanueva, *J. Appl. Phys.* **2004**, *95*, 561.

[11] D. V. Danilov, O. F. Vyvenko, N. A. Sobolev, V. I. Vdovin, A. S. Loshachenko, E. I. Shek, P. N. Aruev, V. V. Zabrodskiy, *SSP.* **2015**, *242*, 368.

[12] D. V. Danilov, O. F. Vyvenko, N. A. Sobolev, V. I. Vdovin, A. S. Loshachenko, E. I. Shek, P. N. Aruev, V. V. Zabrodskiy, *Solid State Phenomena*, **2016**, *242*, 368.

[13] D. Danilov, O. Vyvenko, A. Loshachenko, B. Ber, D. Kasantsev, N. Sobolev, *Phys. Status Solidi C* **2017**, *20*, 1700114.

[14] D. Danilov, O. Vyvenko, M. Trushin, A. Loshachenko, N. Sobolev, *J. Phys. Conf. Ser.* **2019**, *1190*, 012016.

[15] D. Danilov, O. Vyvenko, A. Loshachenko, N. Sobolev, *Phys. Status Solidi A* **2019**, *216*, 1900327.

[16] D. Kot, G. Kissinger, M. A. Schubert, M. Klingsporn, A. Huber, A. Sattler, *Phys. Status Solidi RRL* **2015**, *9*, 405.

[17] G. Kissinger, M. A. Schubert, D. Kot, T. Grabolla, *ECS Trans.* **2016**, *75*, 81.

[18] V. V. Kveder, Yu. A. Osipyan, W. Schröter, G. Zoth, *Phys. Status Solidi A* **1982**, *72*, 701.

[19] P. Omling, E. R. Weber, L. Montelius, H. Alexander, J. Michel, *Phys. Rev. B.* **1985**, *32*, 6571.

[20] D. P. Kennedy, P. C. Murley, W. Kleinfelder, *IBM J. Res. Dev.* **1968**, *12*, 399.

[21] C. P. Wu, E. C. Douglas, C. W. Mueller, *IEEE Trans. Electron Devices* **1975**, *22*, 319.

[22] W. C. Johnson, P. T. Panousis, *IEEE Trans. Electron Devices* **1971**, *18*, 965.

[23] P. V. Gray, D. M. Brown, *Appl. Phys. Lett.* **1966**, *8*, 31.

[24] M. J. Kirton, M. J. Uren, *Appl. Phys. Lett.* **1986**, *48*, 1270.

[25] D. Vuillaume, R. Bouchakour, M. Jourdain, J. C. Bourgoin, *Appl. Phys. Lett.* **1989**, *55*, 153.